Synthesis of Butyl Acrylate in a Fixed-Bed Adsorptive Reactor over Amberlyst 15

Dânia S. M. Constantino, Carla S. M. Pereira, Rui P. V. Faria, Alexandre F. P. Ferreira, José M. Loureiro, and Alírio. E. Rodrigues

Laboratory of Separation and Reaction Engineering (LSRE), Faculdade de Engenharia, Universidade do Porto, Porto 4200-465, Portugal

DOI 10.1002/aic.14701

Published online December 16, 2014 in Wiley Online Library (wileyonlinelibrary.com)

The butyl acrylate synthesis from the esterification reaction of acrylic acid with 1-butanol in a fixed-bed adsorptive reactor packed with Amberlyst 15 ion exchange resin was evaluated. Adsorption experiments were carried out with non-reactive pairs at two temperatures (323 and 363 K). The experimental results were used to obtain multicomponent adsorption equilibrium isotherms of Langmuir type. Reactive adsorption experiments using different feed molar ratios and flow rates were performed, at 363 K, and used to validate a mathematical model developed to describe the dynamic behavior of the fixed-bed adsorptive reactor for the butyl acrylate synthesis. Due to the simultaneous reaction and separation steps, it was possible to obtain a butyl acrylate maximum concentration 38% higher than the equilibrium concentration (for an equimolar reactants ratio solution as feed at a flow rate of 0.9 mL min^{-1} and 363 K) showing that sorption-enhanced reaction technologies are very promising for butyl acrylate synthesis. © 2014 American Institute of Chemical Engineers *AIChE J*, 61: 1263–1274, 2015

Keywords: butyl acrylate, Amberlyst 15 resin, esterification, Langmuir isotherm, reactive chromatography

Introduction

The synthesis of butyl acrylate (BAc) was the subject of many studies, in the last years, due to its multiple areas of application. This compound is an acrylate monomer with molecular formula $CH_2{=}CHCOO(CH_2)_3CH_3$, which has been referred as precursor of several products, such as adhesives[1] (including PSAs),[2,3] varnishes, finishers of papers, and textiles.[4] It has been also applied in the production of coatings and inks, sealants, plastics, elastomers,[5] and it has been mostly used to produce copolymers.[6–10]

BAc is usually produced by an equilibrium limited reaction between acrylic acid (AAc) and *n*-butanol, in acidic medium, having water as by-product, according to Figure 1.

This system presents a complex thermodynamic behavior since, according to Niesbach et al.,[11] it has five azeotropes: two homogeneous and three heterogeneous. Furthermore, during this esterification reaction, there is a high risk of polymerization, mainly at high temperatures.[12–14] According to several research works,[12,14,15] the addition of an inhibitor helps to avoid the polymerization step; phenothiazine (Ptz) and hydroquinone monomethyl ether have been the most commonly used inhibitors; however, in a recent study,[12] the researchers concluded that Ptz is the most effective one.

These limitations in the production process of BAc led to many research studies to improve the conventional process in terms of cost and environmental issues, which is based on a homogeneous catalyzed multistage process using two reactors and three distillation columns for the recovery of the reactants and the purification of the desired product.[12]

In the last years, process intensification is a subject that has been explored in chemical engineering research. One important example of process intensification is the multifunctional reactors, where reaction and separation steps are integrated into a single equipment, usually known as reactive separations. The reactive separation technologies, when applied to equilibrium-limited reactions, allow overtaking the equilibrium conversion by continuously removing at least one of the products from the reaction medium. These type of reactors lead to smaller, cleaner and more energy-efficient processes than the conventional ones.[16,17]

Chromatographic reactors and reactive distillation (RD) are the most studied intensification processes. RD was investigated to improve several conventional processes, including the BAc production. Schwarzer and Hoffman[18] experimentally studied the reaction equilibrium and kinetics and they used those data to simulate a process to produce BAc using a catalytic tubular reactor and a RD column. They concluded that attaching a phase separator above the condenser had an advantageous effect on the BAc yield because water is removed selectivity at the top of the column favoring the BAc production in terms of equilibrium and kinetics. They also observed in some simulations an unstable reaction mixture at the top of the column that could lead to a phase separation affecting the properties of the column's products

Additional Supporting Information may be found in the online version of this article.

Correspondence concerning this article should be addressed to A. E. Rodrigues at arodrig@fe.up.pt.

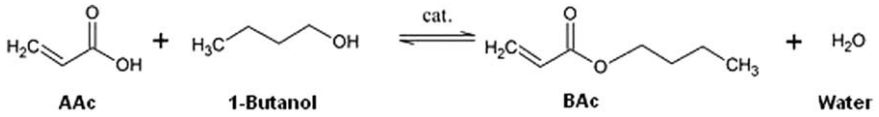

Figure 1. Esterification reaction of acrylic acid with 1-butanol.

streams, which should be avoided. Zeng et al.,[4] theoretically investigated the design and control of a RD column with an overhead decanter using the data of Schwarzer and Hoffman.[18] It was achieved a high purity 99.83 mol % BAc product at the bottom of the RD column and they concluded that it is better to operate the system at a point with slight imbalance of the stoichiometric feed ratio to achieve strong open-loop sensitivity for the RD column system. Niesbach et al.,[11] besides a theoretical assessment, presented the experimental synthesis of BAc using RD evaluating different parameters like temperature, pressure, and the stability of the catalyst among others and taking into account for the first time the polymerization risk. An intensive study about preventing the polymerization reactions in this process was recently published by the same group.[12] It was concluded that Ptz is more effective than hydroquinone monomethyl ether. Furthermore, an optimization of the BAc synthesis process in a RD column at industrial scale using a nonequilibrium stage model was also studied by this group, achieving a significant reduction of production costs, by the implementation of a decanter at the top of the column (allowing recycling of unused reactants), comparing with a single RD column as well as with the conventional process.[19]

In the chromatographic reactors, the separation process is made by adsorption while the reaction step occurs, which can be advantageous over RD for complex molecules that are difficult to separate by evaporation processes.[20] Moreover, chromatographic reactors are operated at lower temperatures than RD being, in principle, preferable to prevent polymerization reactions.

Many studies have been focused on heterogeneous catalysts for the esterification reaction between AAc and *n*-butanol[11,18,21–26] to overcome the environmental drawbacks associated with homogeneous catalysts as well as to facilitate their separation from the final product. It is known that ion exchange resins are active catalysts for esterification reactions. One example is the Amberlyst 15 resin (A15), which was, recently, used in a kinetic study of the BAc system with good results in batch conditions.[27] Furthermore, A15 was already successfully applied in simulated moving bed reactor (SMBR)-based processes for other systems,[28–30] showing high selectivity for water adsorption, being very attractive for BAc synthesis in chromatographic reactors.

The SMBR is a technology developed some years ago that consists in several chromatographic reactors connected in series forming a closed loop which can be operated in a continuous mode. In spite of the good results attained for the production of other compounds involving equilibrium-limited reactions, as diethylacetal,[31] 1,1-dimethoxyethane,[32] ethyl lactate,[28] 1,1-dibutoxyethane,[33] and ethyl acetate,[29] by SMBR, this technology was never evaluated for the production of BAc.

This work aims to study the synthesis of BAc in a fixed-bed adsorptive reactor (FBAR) as a very important step to determine the best conditions to implement a future SMBR process for this system using A15 as catalyst and adsorbent. To assess the performance of this type of reactors, the knowledge of basic data, as adsorption and reaction kinetics on the A15 resin, is crucial. The BAc reaction kinetics in a batch reactor in the presence of A15 was already studied.[27] In this work, an adsorption study with binary mixtures in the absence of reaction was performed, at 323 and 363 K, to obtain the multicomponent adsorption parameters. Then, the kinetic and adsorption data were used in a mathematical model developed to describe the synthesis of BAc in a FBAR, which was validated by reactive adsorption experiments conducted under different conditions.

Experimental

Chemicals and materials

The chemicals used in the adsorption/reaction experiments were *n*-butanol ($\geq$99.9 wt %) from Fisher Scientific, AAc ($\geq$99 wt %) and BAc ($\geq$99.5 wt %) from Acros Organics. AAc and BAc were provided stabilized with inhibitor (about 200 and 20 ppm of hydroquinone monomethyl ether [MeHQ] in AAc and in BAc, respectively). The additional inhibitor used in this study was Ptz (99 wt %), also from Acros Organics. Isopropanol ($\geq$99.9 wt %) from Fisher Scientific was used as solvent in the chromatographic analysis.

A15 resin was used as catalyst and adsorbent. This is a highly crosslinked polystyrene-divinylbenzene ion exchange resin functionalized with sulfonic groups, which swells selectively in contact with a liquid phase multicomponent mixture, especially with polar species.[34] This fact depends on the interactions between the fluid and the resin as well as on the amount of crosslinks.[35] In this work, the swelling ratios were measured at 323 K for all compounds of the system under study. The values are 1.55, 1.54, 1.35, 1.08 for water, *n*-butanol, AAc and BAc, respectively. Thereby, it is possible to conclude that A15 has the following decreasing affinity order: water, *n*-butanol, AAc, and BAc, which is in accordance with the species polarity. The concentration of active sites of this resin is 4.7 meq H^+ g^{-1} (dry matter), its surface area is 53 m^2 g^{-1}, its average radius is 372.5 μm, and its particle porosity is 0.36.[20] The catalyst/adsorbent was first washed with deionized water and then with ethanol. Then, it was dried at 90°C and prior to the packing the resin was immersed in *n*-butanol.

Analytical method

All samples collected were analyzed (at least two times) in a Shimadzu—GC 2010 Plus gas chromatograph equipped with flame ionization and thermal conductivity detectors. The compounds were separated using a silica capillary column (CPWax57CB, 25 m $\times$ 0.53 mm ID, film thickness of 2.0 μm). Helium N50 was used as the carrier gas at a flow rate of 3.9 mL min^{-1}. The linear velocity was set to 30 cm s^{-1}

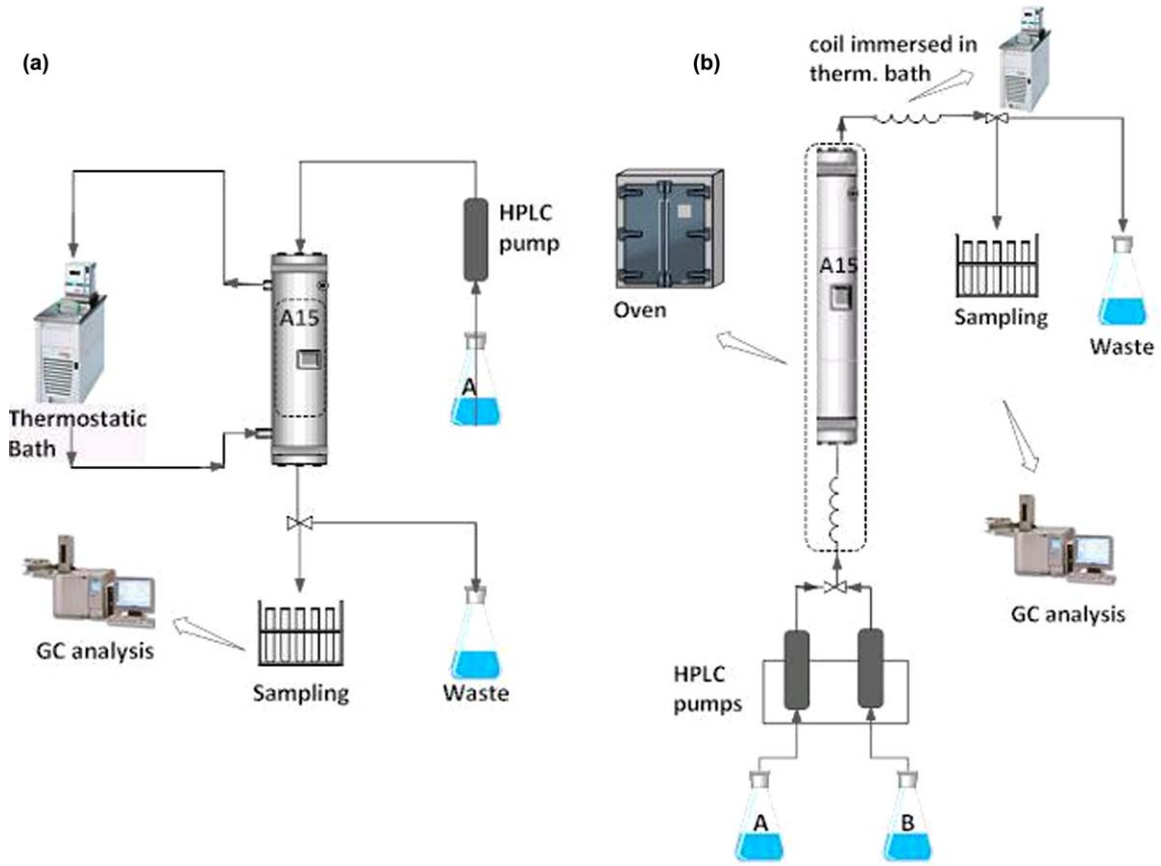

Figure 2. Experimental set up: (a) jacket glass column used at 323 K (top-down flow direction); (b) stainless steel column used at 363 K (bottom-up flow direction).

[Color figure can be viewed in the online issue, which is available at wileyonlinelibrary.com.]

and the injection volume used was 0.8 μL with a split ratio of 15. The temperature of the injector and of the Thermal Conductivity Detector (TCD) was set to 523 K while the temperature of the Flame Ionization Detector (FID) was set to be 573 K. The initial column temperature was 393 K for 4.3 min, the temperature was then increased at 60 K min^{-1} up to 473.15 K remaining constant for the following 17 min. Isopropyl alcohol (isopropanol) was used as solvent. The global associated uncertainty of the measured molar fractions was ≤ 0.05.

Experimental set up and procedure

The experiments at 323 K were carried out in a laboratory-scale jacketed glass column, which was kept at the desired temperature by a thermostatic bath, while the experiments at 363 K were performed in a stainless steel column able to withstand higher temperatures placed inside an oven (Figure 2). The main differences between the set ups used and shown in the Figure, besides the columns, are that the sampling is performed manually at 323 K and automatically at 363 K and on the left side set up only one HPLC pump was used to feed the column while on the right side set up one HPLC pump was used for the adsorption mixture and another for the regeneration step, avoiding the need to purge the system. Both columns were packed with the sulfonic acid ion exchange resin A15 and their characteristics can be seen in Table 2.

Tracer experiments were carried out by pulse injections of a Dextran solution (15 kg m^{-3}) in water, since Dextran is insoluble in *n*-butanol. Samples of 0.2 cm^3 were injected at different flow rates (5, 7.5, and 10 mL min^{-1}) using water as eluent and the column outlet concentration was monitored using a UV–VIS detector (Gilson, Model 115) at 300 nm. At least, three runs were performed for each flow rate to check the stoichiometric time reproducibility of the experimental curves.

The adsorption experiments were performed by feeding to the fixed-bed column different binary mixtures of known composition of a reactant and a product of the esterification reaction, at constant temperature and feed flow rate. To obtain the breakthrough curves, small samples were collected at the column outlet, at periodic time intervals, and analyzed by gas chromatography according to the analytical method described above. The reactive adsorption experiments were performed in a similar way, but now by feeding reactive mixtures comprising *n*-butanol and AAc, to the fixed-bed column. In both cases, the experiments proceeded until no changes were observed in the outlet stream composition.

Since BAc and AAc have high risk of polymerization at high temperatures, previous tests were performed using binary mixtures of these compounds (AAc/water and AAc/BAc) in batch conditions over A15 resin at the same work temperatures during 8 h. It was not observed the formation of any by-products at 323 K; however, at 363 K, two new peaks were observed in the corresponding chromatograms, which can be butyl 3-butoxypropanoate or butyl 3-acryloxypropanoate, according to the literature[21] (3-butoxypropionic acid and butyl hydroxypropanoate—also possible by-products—were tested and excluded as possibilities). Nevertheless, the area ratios observed were less

than 5% (A_i/A_{total}). Anyway, some adsorption experiments were repeated using Ptz as inhibitor to check its effect in the adsorption profile. The amount of Ptz used was 1000 ppm as suggested by Niesbach et al.[12]

Mathematical model

A mathematical model was developed to predict the internal concentration profiles or the concentration histories of a FBAR applied in the synthesis of BAc using the A15 resin as catalyst and water selective adsorbent, which takes into account the following assumptions:

1. Isothermal operation;
2. Constant bed and packing porosities;
3. Plug flow model with axial dispersion but negligible radial dispersion;
4. Velocity variations due to changes in the bulk composition;
5. Mass transfer described by the linear driving force model;
6. Multicomponent adsorption equilibrium described by extended Langmuir isotherm model.

The bulk fluid and pellet mass balances to component i are given by Eqs. 1 and 2, respectively

$$\frac{\partial C_i}{\partial t}+\frac{\partial (uC_i)}{\partial z}+\frac{(1-\varepsilon)}{\varepsilon}\frac{3}{r_p}K_{L,i}\left(C_i-\bar{C}_{p,i}\right)=D_{ax}\frac{\partial}{\partial z}\left(C_T\frac{\partial x_i}{\partial z}\right) \tag{1}$$

$$\frac{3}{r_p}K_{L,i}\left(C_i-\bar{C}_{p,i}\right)=\varepsilon_p\frac{\partial \bar{C}_{p,i}}{\partial t}+\left(1-\varepsilon_p\right)\frac{\partial \bar{q}_i}{\partial t}-\frac{v_i\rho_b}{1-\varepsilon}r\left(\bar{C}_{p,i}\right) \tag{2}$$

where $K_{L,i}$, C_i, and $\bar{C}_{p,i}$ represent the global mass-transfer coefficient, the bulk concentration and the average concentration in the particle pores of component i, respectively. x_i is the component molar fraction and C_T the total concentration in the liquid phase; u is the interstitial velocity, ε the bed porosity, and D_{ax} is the axial dispersion coefficient, which was obtained from the Peclet number, according to Eq. 3; z is the axial dimension along the bed, r is the particle radius, and t is time.

The interstitial fluid velocity variation is given by Eq. 4, which was obtained from the total mass balance

$$P_e=\frac{uL_b}{D_{ax}} \tag{3}$$

$$\frac{du}{dz}=-\frac{(1-\varepsilon)}{\varepsilon}\frac{3}{r_p}\sum_{i=1}^{NC}k_{L,i}V_{M,i}\left(C_i-\bar{C}_{p,i}\right) \tag{4}$$

where $V_{M,i}$ is the molar volume of component i and NC is the number of compounds.

In Eq. 2, ρ_b is the bulk density, ε_p is the particle porosity, $\overline{q}_i$ is the average adsorbed phase concentration of species i in equilibrium with $\bar{C}_{p,i}$, v_i is the stoichiometric coefficient of component i and r is the kinetic rate of the chemical reaction.

The adsorption equilibrium of component i is described by the multicomponent Langmuir adsorption equilibrium isotherm

$$q_i=\frac{Q_iK_i\overline{C}_{p,i}}{1+\sum_{j=1}^{NC}K_j\overline{C}_{p,j}} \tag{5}$$

where Q_i is the monolayer capacity and K_i is the equilibrium constant for component i.

It is known that, for thermodynamic consistency, the maximum molar capacity of an adsorbent should be the same for all species to follow the Langmuir equilibrium model assumption. However, this assumption is not verified for molecules of very different sizes.[31] Therefore, in some scientific works, it is assumed a constant monolayer capacity in terms of mass[36] or in terms of volumes.[28] In this work, it was considered a constant volumetric monolayer capacity for all species, Q_v, which is given by $Q_v=Q_i\times V_{M,i}$. This assumption allowed reducing the adjustable adsorption parameters from 8 (one molar monolayer capacity and one equilibrium constant for each species) to 5 (one volumetric monolayer capacity for all species and one equilibrium constant for each species), at each temperature.

The rate of chemical reaction is given by the following equation[27]

$$r=k_c\frac{a_Aa_B-\frac{a_Ca_D}{K_{eq}}}{\left(1+K_{s,D}a_D\right)^2} \tag{6}$$

where in a_i are the species activities (calculated using the UNIFAC model), the subscripts A, B, C, and D refer to *n*-butanol, AAc, BAc, and water, respectively, and k_c, $K_{s,D}$, and K_{eq} are the kinetic constant, the water adsorption constant, and the thermodynamic equilibrium constant, respectively, which are equal to[27]

$$k_c\left(\text{molg}_{A15}^{-1}\text{min}^{-1}\right)=1.52\times 10^7\times\exp\left(-\frac{66988}{RT}\right) \tag{7}$$

$$K_{s,D}=1.589 \tag{8}$$

$$K_{eq}=\exp\left(\frac{-1490}{T(K)}+7.21\right) \tag{9}$$

Initial and Danckwerts boundary conditions are given by Eqs. 10–13, where the subscripts F and 0 represent the feed and initial condition, respectively

$$t=0 \qquad C_i=\bar{C}_{p,i}=C_{i,0} \tag{10}$$

$$z=0 \qquad uC_i-D_{ax}\,C_T\frac{\partial x_i}{\partial z}\bigg|_{z=0}=uC_{i,F} \tag{11}$$

$$z=0 \qquad u=u|_{z=0} \tag{12}$$

$$z=L \qquad \frac{\partial C_i}{\partial z}\bigg|_{z=L}=0 \tag{13}$$

Mass-transfer parameters

In this model, a global mass-transfer coefficient was considered that combines external and internal mass-transfer coefficients, k_e and k_i, respectively, according to the resistances-in-series model given by the following equation

$$\frac{1}{K_L}=\frac{1}{k_e}+\frac{1}{\varepsilon_pk_i} \tag{14}$$

The internal mass-transfer coefficient was estimated by Glueckauf Eq. 15[37] while the external mass-transfer coefficient was estimated by the Wilson and Geankopolis correlation,[38] expressed by Eq. 16

Table 1. Characteristics of the Fixed-Bed Columns

Characteristic/column	Jacketed glass	Stainless steel
Length of the column, L(cm)	12.0	35.1
Internal diameter of the column, D_i (cm)	2.6	1.95
A15 weight (g)	24.9	41.0
Bulk density ρ_b(g dm^{-3})	390.8	391.0

$$k_i = \frac{5D_m/\tau}{r_p} \tag{15}$$

$$Sh_p = \frac{1.09}{\varepsilon}\left(Re_p S_c\right)^{0.33} \quad 0.0015 < \mathrm{Re}_p < 55 \tag{16}$$

where Sh_p and Re_p are the Sherwood and Reynolds numbers relative to the particle, respectively, described by Eqs. 17 and 18. The Schmidt number, Sc, was determined according to Eq. 19

$$Sh_p = \frac{k_e d_p}{D_m} \tag{17}$$

$$Re_p = \frac{\rho d_p u}{\eta} \tag{18}$$

$$S_c = \frac{\eta}{\rho D_m} \tag{19}$$

The infinite dilution diffusivities were estimated by the Scheibel correlation[39]

$$D^0_{A,B} = \frac{8.2\times10^{-8}T}{\eta_B V_{M,A}^{1/3}}\left[1+\left(\frac{3V_{M,B}}{V_{M,A}}\right)^{2/3}\right] \tag{20}$$

where $D^0_{A,B}$ is the diffusion coefficient for a dilute solute A into a solvent B and η_B is the viscosity of pure solvent B.

Vignes equation,[40] based on coefficients at infinite dilution, was used to predict the diffusion coefficient in concentrated solutions for binary systems

$$D_{B,A} = D_{A,B} = (D^0_{A,B})^{x_2}(D^0_{B,A})^{x_1} \tag{21}$$

The diffusion coefficient for multicomponent concentrated solutions was determined by the Perkins and Geankoplis[41] mixing rule

$$D_{A,m}\eta_m^{0.8} = \sum_{\substack{i=1\\ i\neq A}}^{n} x_i D^0_{Aj}\eta_i^{0.8} \tag{22}$$

where η_m is the viscosity of the mixture and η_i is the viscosity of the component i.

Numerical solution

The numerical solution of this problem was obtained using the commercial software general PROcess Modelling System version 3.5.3, using a method of orthogonal collocation in finite elements; to this end, the axial dimension of the bed was discretized in 21 finite elements with two interior collocation points in each finite element and the Differential-Algebraic equation SOLVer (DASOLV) integrated solver was used to solve the remaining system of ordinary differential equations in time. For all simulations, a tolerance of 10^{-5} was used.

Results and Discussion

Fixed-bed column characterization

Tracer experiments were performed at 323 K (shows as Supporting Information) to characterize the glass fixed-bed column in terms of Peclet number and bed porosity. These experiments were carried out by pulse injections of a Dextran solution, since its molecules are large enough to avoid entering in the resin particles pores. The theoretical results were obtained using the proposed fixed-bed model without the reaction, adsorption and mass-transfer terms, since these phenomena do not occur in the tracer experiments.

The bed porosity and the Peclet number were calculated according to Eqs. 24 and 25, respectively, where $\bar{t}$ is the mean residence time and σ^2 is the variance of the residence time distribution curve. The results obtained are presented in Table 2

$$E(t) = \frac{C_{out}(t)}{\int_0^\infty C_{out}(t)dt} \tag{23}$$

$$\varepsilon = \frac{\bar{t}}{V_b/Q} = \frac{\int_0^\infty tE(t)dt}{V_b/Q} \tag{24}$$

$$Pe = \frac{2\bar{t}^2}{\sigma^2} = \frac{2\bar{t}^2}{\int_0^\infty (t-\bar{t})^2 E(t)dt} \tag{25}$$

Regarding to the stainless steel column used for experiments performed at 363 K, despite its different dimensions (see Table 1, where the fixed-bed columns characteristics are presented), the bulk density is almost the same, which implies the same bed porosity (≈0.4). The Pe number was determined from the following empirical correlation valid for liquids in packed beds[42]: $\varepsilon Pe_p = 0.2 + 0.011 Re_p^{0.48}$ (subscript p corresponds to the particle), where $Pe_p = Ped_p/L_b$. The Pe number obtained from this correlation was 226. To validate the correlation, the same was applied to calculate the Pe number of the glass column. The correlation gives a Pe equal to 82, while from the tracer experiments an average value of 110 was determined (Table 2).

Adsorption isotherms

The multicomponent adsorption equilibrium was studied at two temperatures, 323 and 363 K. The breakthrough curves of nonreactive pairs were measured in accordance to what was described in Experimental Set Up and Procedure section, to evaluate the A15 performance in terms of adsorption capacity and selectivity for all compounds of the system under study. The possible binary mixtures to perform the breakthrough experiments in the absence of reaction are: *n*-butanol/water, *n*-butanol/BAc, AAc/water, and AAc/BAc.

Table 2. Tracer Experiments Results at 323 K

Run	Q (mL min^{-1})	$\bar{t}$ (min)	ε	Pe	σ^2 (min^2)
1	5.0	4.87	0.42	107	0.446
2	7.5	3.27	0.41	109	0.215
3	10.0	2.45	0.41	116	0.199

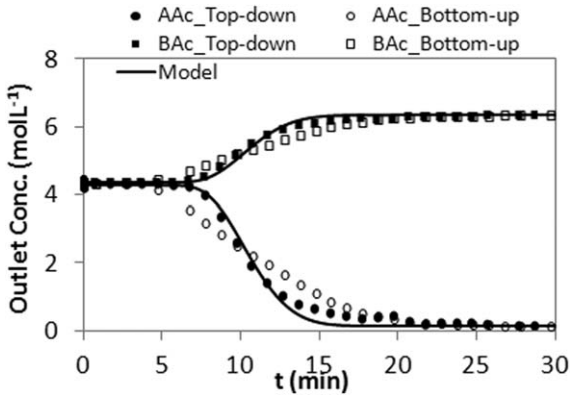

Figure 3. Breakthrough curves for BAc displacing a BAc/AAc mixture (50/50 mol %) using different feed configuration: top-down (■/•) and bottom-up (□/○).

Preliminary studies

It has been referred in the literature[28,31,43] that it is extremely important to set the correct liquid flow direction, which should be based on the different species densities; bottom-up or top-down direction must be used to ensure that the component above the front is less dense than the component below the front. This condition avoids a possible axial backmixing phenomenon driven by natural convection.[31] An example is shown in Figure 3, where the results of two adsorption experiments performed at the same conditions but using opposite feed flow directions are presented. It can be observed in Figure 3 that the use of the bottom-up configuration results in more dispersive curves than when the correct configuration (top-down direction since a less dense mixture is being fed) is used. In all the experiments, the correct feed flow direction was considered, taking into account the densities of the species, which, at 363 K, are 746, 823, 963, and 970 kg m^{-3}, for *n*-butanol, BAc, water, and AAC, respectively.

The effect of the presence of inhibitor was also studied by performing the same breakthrough experiment with and without Ptz. According to the suggested by Niesbach et al.,[12] to suppress the formation of by-products, it was ensured an amount of 1000 ppm of Ptz along the column bed during the experiment. The breakthrough curves obtained are shown in Figure 4, where it is visible that the inhibitor has no significant effect on the results.

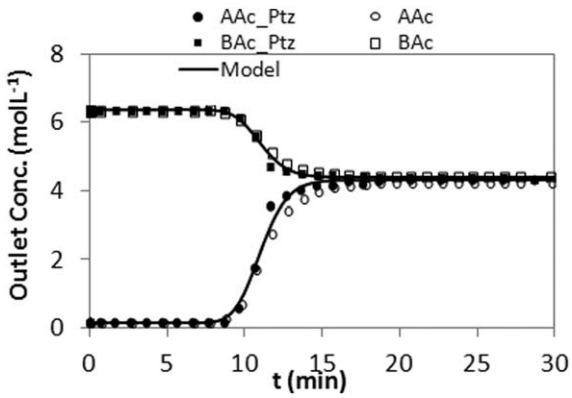

Figure 4. Breakthrough curves for a mixture BAc/AAc (50/50 mol %) displacing a BAc solution using or not inhibitor: with Ptz (■/•) and without Ptz (□/○).

Adsorption experiments

The adsorption results were used to calculate the experimental number of moles adsorbed/desorbed according to Eq. 26. Then, the parameters of the multicomponent Langmuir adsorption isotherms (Eq. 5) were determined by minimizing the difference between experimental and theoretical values (determined by Eq. 27), according to Eq. 28, and applying a Jackknife methodology.[44] The same procedure was applied for the results at 323 K

$$n_{\text{exp}} = \zeta Q \int_0^{\infty} [C_{\text{F}} - C_{\text{out}}(t)]dt \tag{26}$$

$$n_{\text{the}} = \zeta\{([\varepsilon + (1-\varepsilon)\varepsilon_{\text{p}}](C_{\text{F}} - C_0) + (1-\varepsilon)(1-\varepsilon_{\text{p}})[q(C_{\text{F}}) - q(C_0)])/V\} \tag{27}$$

where $\zeta = 1$ for adsorption step and $\zeta = (-1)$ for desorption step

$$F_{\text{obj}} = \sum_{k=1}^{\text{NE}} \left[\left(n_{\text{exp}}^{\text{ads}} - n_{\text{the}}^{\text{ads}} \right)^2 + \left(n_{\text{exp}}^{\text{des}} - n_{\text{the}}^{\text{des}} \right)^2 \right] \tag{28}$$

The final adsorption parameters as well as the respective molar volumes at 323 and 363 K are summarized in Table 3.

The breakthrough curves for all the possible binary mixtures obtained using the correct liquid flow direction and without inhibitor (except the inhibitor already present in the acquired AAc and BAc purchased), at 363 K, are shown in Figures 5–8, while the adsorption results at 323 K are shown as Supporting Information.

The experimental results are generally well predicted by the mathematical model using the optimized adsorption parameters presented in Table 3. For the pair *n*-butanol/water, Figure 5, the mean deviation obtained between experimental and theoretical amounts of *n*-butanol adsorbed are 1.1, 1.7, and 0.2% for the results presented in (a), (b), and (c), respectively. For water, deviations of 2.0% (a) and 0.9% [(b) and (c)] between the experimental and theoretical desorbed amounts were observed. Regarding to the *n*-butanol/BAc pair (Figure 6), the differences obtained between the experimental amount adsorbed of BAc and the one predicted were 0.7, 7.9, and 1.5% for the experiments shown in (a), (b), and (c), while for the amount desorbed of *n*-butanol, the mean deviations obtained were 0.6, 8.0, and 0.8%, respectively. The higher deviations between the experimental results and the model predictions are observed for AAc/water mixture (Figure 7); a mean deviation of about 20% for the amount adsorbed/desorbed of AAc/water were observed, except for the experiment (b) for which it was found a mean deviation of 6.4% between the experimental and theoretical number of moles for both species. This large deviation might be caused by some polymerization of AAc in the column despite the fact that in the experiments performed using AAc, the concentration of this species was never higher than 50 mol %, because of the risk of polymerization and also to avoid possible corrosion of the experimental set up components such as the peristaltic pumps. Nevertheless, it is known that AAc tends to polymerize at high temperatures.[12,14,15] Indeed, after the adsorption experiments performed with this binary mixture, the column was opened and it was observed

Table 3. Adsorption Parameters Over A15 Resin and Molar Volume at 323 and 363 K

	Q_V (mL $L^{-1}_{wet\ solid}$)		K (L mol^{-1})		V_M (mL mol^{-1})	
Component	323 K	363 K	323 K	363 K	323 K	363 K
n-Butanol	462.0 ± 2.0	452.5 ± 10.8	6.90 ± 1.51	7.07 ± 2.59	94.71	99.38
Water			48.74 ± 7.39	22.74 ± 8.09	18.24	18.71
BAc			2.67 ± 0.30	1.94 ± 0.34	147.65	155.65
AAc			3.51 ± 0.32	1.90 ± 0.45	70.85	74.31

the presence of an apparently viscous polymer like a colorless gel with elastic properties in the bulk. However, no significant amount of other species were detected in the liquid phase (less than 5% of A_i/A_{total}) as already reported by other authors.[14] For the pair BAc/AAc, both species with high risk of polymerization, good results were obtained as can be observed in Figure 8, resulting mean deviations of 0.2 (a), 3.0 (b), 12.3 (c), and 8.0 % (d) between experimental and predicted amounts desorbed of BAc and 0.9 (a), 1.9 (b), 11.2 (c), and 7.0 % (d) for the amounts adsorbed of AAc. Accordingly, this fact leads to conclude that, besides the high temperature, water had the main role in the formation of the polymer observed in the experiments with AAc/water, like it happens in the hydrogel synthesis. This kind of polymers, as polyacrylic acid, are formed in the aqueous phase and they have water holding capacity and permeability as important characteristics, leading to the formation of a network that swells.[45] This process leads to believe that there was a change in the bulk conditions which hampered the passage of the fluid through the bed, delaying the breakthrough curves in relation to the predicted by the model. Nevertheless, the experimental adsorption results are overall well described by the considered mathematical model.

Fixed-bed adsorptive reactor

A simulation study was performed to predict the performance of the FBAR, at 323 and 363 K, when an equimolar mixture of reactants (AAc and *n*-butanol) is fed at 1 mL min^{-1} to the fixed-bed column (stainless steel) saturated with *n*-butanol. It was concluded that, at 323 K, the conversion achieved under these conditions is small due to the low reaction rate. At steady state, the conversion obtained is 17%, which is significantly smaller than that attained in a batch reactor under the same conditions (56%). Indeed, at this temperature, the reaction equilibrium conversion for an equimolar mixture of AAc and *n*-butanol can only be achieved for a FBAR space time of approximately 186 min.

To increase the reaction rate, attain higher conversions and, consequently, better performance in the BAc production, the reaction plus adsorption experiments were conducted at 363 K.

A first experiment ($FBAR_1$) was performed by feeding a mixture comprising AAc and *n*-butanol in the stoichiometric amount, at a flow rate of 1.3 mL min^{-1}, to the stainless steel column packed with A15 saturated with *n*-butanol (Figure 9). As soon as the reactive mixture enters the column it is adsorbed by A15 and starts to react producing BAc and water in stoichiometric amounts. As shown in Figure 9, BAc

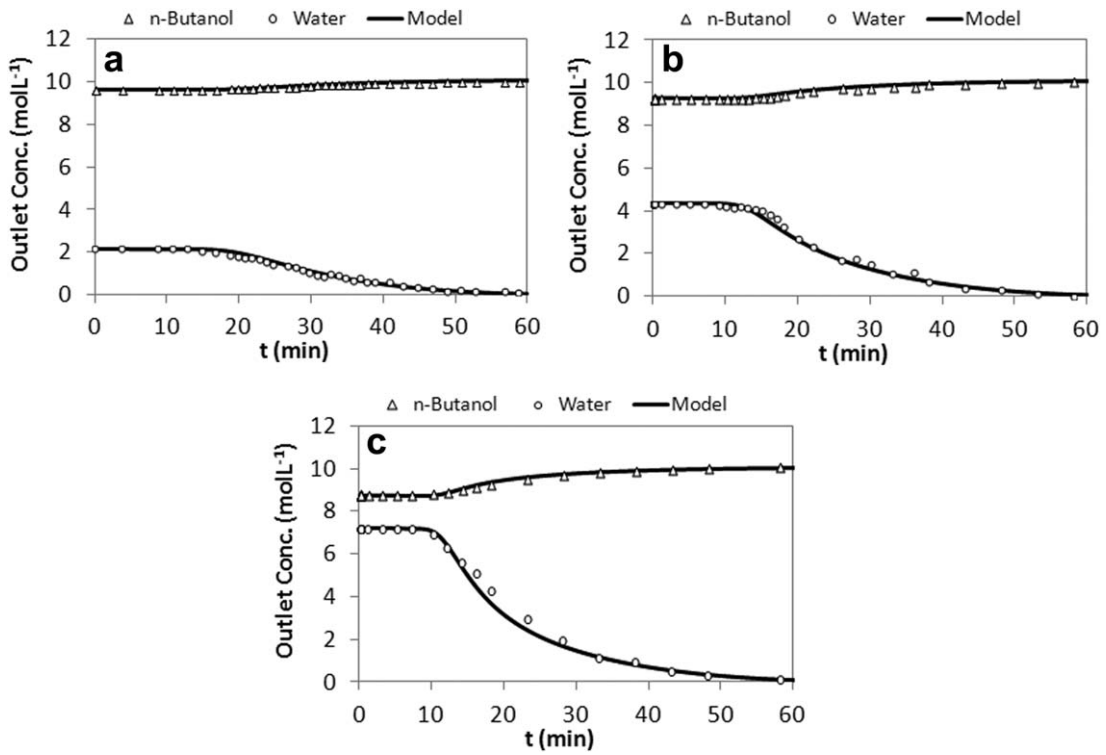

Figure 5. Breakthrough curves for *n*-butanol displacing *n*-butanol/water mixtures [80/20 (a), 67/33 (b), and 55/45 (c) mol %] at 7.5 mL min^{-1} and 363 K; top-down direction.

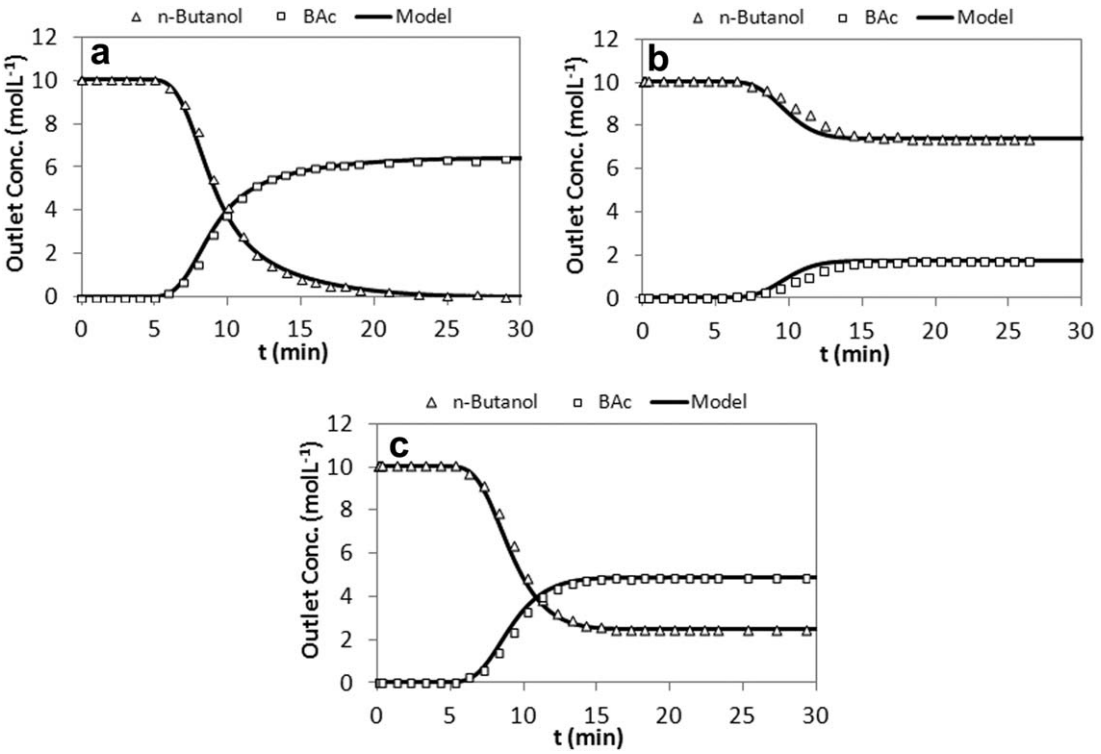

Figure 6. Breakthrough curves for *n*-butanol/BAc mixtures [0/100 (a), 80/20 (b), and 33/67 (c) mol %] displacing *n*-butanol at 7.5 mL min^{-1} and 363 K; bottom-up direction.

is the first eluted species, while water is the last, in accordance with the resin affinity toward these components (BAc is the less adsorbed component; water is the most adsorbed one). The concentration profiles evolution continues until the resin is completely saturated with water. After this, the selective separation of BAc and water is no longer possible, the outlet stream composition remains constant and the FBAR achieves the steady state. A maximum concentration of the desired product (BAc) equal to 5 mol L^{-1}, at approximately 85 min, was achieved, which significantly overcomes

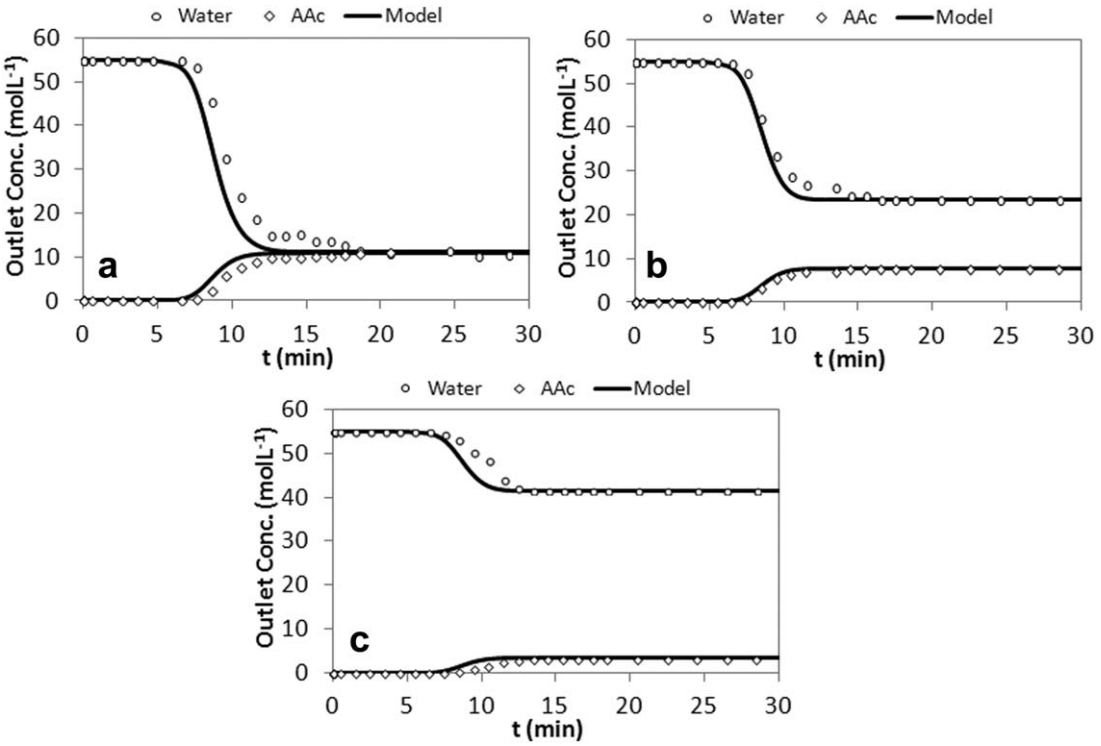

Figure 7. Breakthrough curves for AAc/water mixtures [50/50 (a), 30/70 (b), and 10/90 (c) mol %] displacing water at 7.5 mL min^{-1} and 363 K; bottom-up direction.

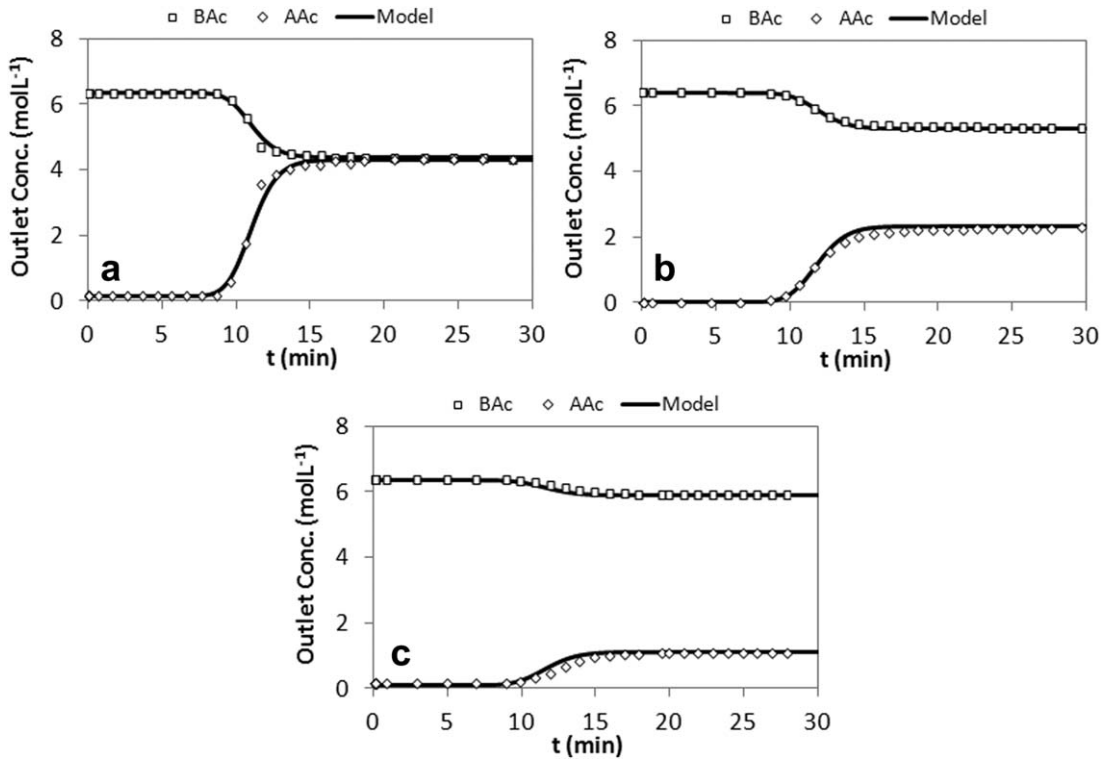

Figure 8. Breakthrough curves for AAc/BAc mixtures [50/50 (a), 35/65 (b), 10/90 (c), and 0/100 mol %] displacing BAc at 7.5 mL min^{-1} and 363 K; bottom-up direction.

the equilibrium concentration that is equal to about 3 mol L^{-1} (represented by a dashed line in Figure 9). This result demonstrates the potential of sorption enhanced reactor technologies, as the FBAR and the SMBR, for the BAc production. After the $FBAR_1$ experiment, a regeneration step was performed by feeding *n*-butanol at a flow rate of 7.5 mL min^{-1} to the column to displace all the adsorbed components. The concentration histories obtained at the fixed-bed column outlet during the regeneration step are shown in Figure 10, where it can be observed that AAc and BAc are completely eluted after 12 min, while water requires about 60 min to be desorbed using, therefore, a significant larger amount of *n*-butanol than the other species. In both reactive and regeneration steps, the model describes reasonably well the experimental results (Figures 9 and 10).

To validate the mathematical model under different conditions, additional reactive adsorptive experiments were performed: $FBAR_2$—an equimolar reactants ratio solution was fed at a flow rate of 0.9 mL min^{-1} (Figure 11) and $FBAR_3$—a mixture with reactants molar ratio 3:1 (*n*-butanol: AAc) was fed at a flow rate of 1.0 mL min^{-1} (Figure 12).

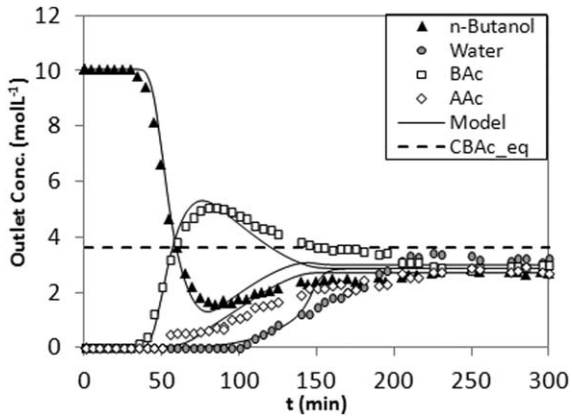

Figure 9. $FBAR_1$—Experimental and simulated concentration histories at the outlet of the fixed-bed adsorptive reactor initially saturated with *n*-butanol and fed with a mixture of AAc/*n*-butanol ($C_{n\text{-butanol,F}} = 5.88$ mol L^{-1} and $C_{AAc,F} = 5.60$ mol L^{-1}); bottom-up feed configuration; $Q = 1.3$ mL min^{-1} and $T = 363$ K.

Dashed line represents the concentration of BAc in equilibrium in batch conditions.

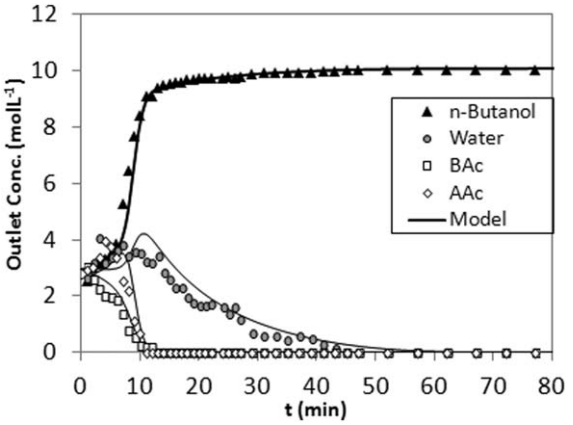

Figure 10. $FBRA_1$_R—Experimental and simulated concentration histories at the outlet of the fixed-bed adsorptive reactor for the regeneration step with *n*-butanol; top-down feed configuration; $Q = 7.5$ mL min^{-1} and $T = 363$ K.

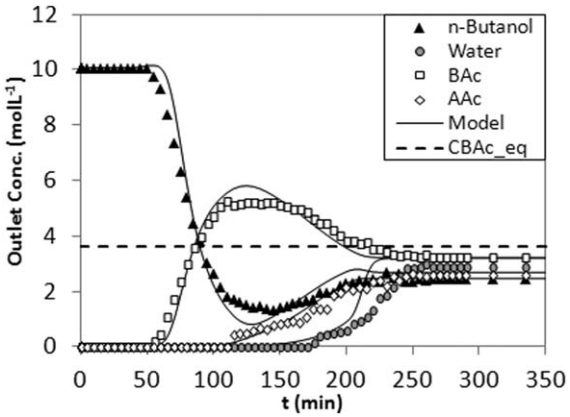

Figure 11. $FBAR_2$—Experimental and simulated concentration histories at the outlet of the fixed-bed adsorptive reactor initially saturated with *n*-butanol and fed with a mixture of AAc/*n*-butanol ($C_{n\text{-butanol,F}} = 5.91$ mol L^{-1} and $C_{AAc,F} = 5.67$ mol L^{-1}); Bottom-up feed configuration; $Q = 0.9$ mL min^{-1} and $T = 363$ K.

Dashed line represents the concentration of BAc in equilibrium in batch conditions.

Once again, in both cases, the column was previously saturated with *n*-butanol. The behavior observed in the species concentration histories at the column outlet shown in Figure 11 is similar to the one described above for the $FBAR_1$. The outlet concentrations of both reactants and products at the steady state should be the same (as in experiment $FBAR_1$). However, this is not observed in the case of the products (water presents a lower concentration than BAc), which might be due to errors associated with the analytical method. Due to the simultaneous reaction and separation steps, in the $FBAR_2$ experiment, it was possible to obtain a BAc maximum concentration 38% higher than the equilibrium concentration. The $FBAR_2$ and $FBAR_3$ experimental results are also reasonably well described by the considered mathematical model as can be seen in Figures 11 and 12, respectively. Nevertheless, the quality of the fittings was determined quantitatively by computing the respective correlation coefficient, R^2_{corr}, according to the following equation

$$R^2_{corr} = 1 - \frac{\sum_{i=1}^{NC}\sum_{j=1}^{NE}\sum_{k=1}^{NP}\left(C^{exp}_{out,i,j,k} - C^{mod}_{out,i,j,k}\right)^2}{\sum_{i=1}^{NC}\sum_{j=1}^{NE}\sum_{k=1}^{NP}\left(C^{exp}_{out,i,j,k} - \bar{C}^{mod}_{out,i}\right)^2} \quad (29)$$

where NC, NE, and NP are the number of compounds, experiments, and data points, respectively. The value obtained for this parameter was 0.975, confirming that the mathematical model implemented describes with good accuracy the concentration histories of all compounds in FBAR experiments.

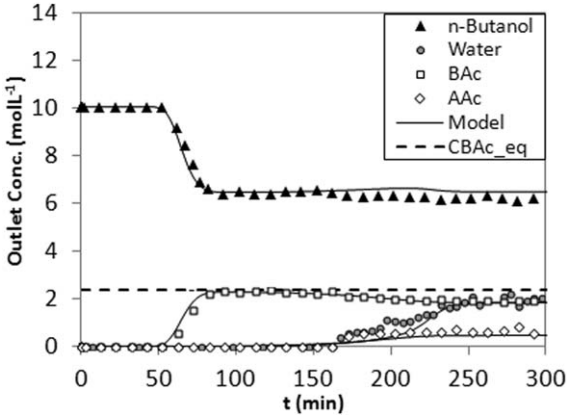

Figure 12. $FBAR_3$—Experimental and simulated concentration histories at the outlet of the fixed-bed adsorptive reactor initially saturated with *n*-butanol and fed with a mixture of AAc/*n*-butanol ($C_{n\text{-butanol,F}} = 8.35$ mol L^{-1} and $C_{AAc,F} = 2.28$ mol L^{-1}); Bottom-up feed configuration; $Q = 1.0$ mL min^{-1} and $T = 363$ K.

Dashed line represents the concentration of BAc in equilibrium in batch conditions.

Conclusions

The feasibility of the BAc production in a FBAR packed with A15 ion exchange resin was assessed.

An adsorption study using nonreactive binary mixtures was performed, at 323 and 363 K, to determine the adsorption parameters of the selected isotherm (multicomponent Langmuir isotherm) at this two temperatures. The resin affinity toward the species involved in BAc synthesis in descending order is: water, *n*-butanol, AAc, and BAc.

Reactive adsorption experiments were also performed under different conditions to validate the proposed mathematical model that considers: isothermal operation, axial dispersion, constant bed volume, and packing (porosity), internal and external mass-transfer resistances, and velocity variations due to changes in the bulk composition. This model is efficient in the prediction of adsorption, reaction, and regeneration steps and it will be an important tool to implement and develop sorption enhanced reaction technologies. This type of reactors is very promising for the sustainable BAc synthesis as proved by the conversions significantly above the equilibrium attained in the FBAR.

Acknowledgments

Financial support for this work was provided by project grant EXCL/QEQ-PRS/0308/2012 and by project PEst-C/EQB/LA0020/2011, financed by FEDER through COMPETE—Programa Operacional Factores de Competitividade and by FCT—Fundação para a Ciência e a Tecnologia, for which the authors are thankful. This work was also cofinanced by QREN, ON2, and FEDER (Project NORTE-07–0124-FEDER-0000007—Multifunctional Reactors/Process Intensification). C.S.M. Pereira acknowledges Fundo Social Europeu (European Social Fund) and Programa Operacional Potencial Humano (Human Potential Operational Programme; FCT Investigator-IF/01486/2013).

Notations

Abbreviations

RD = reactive distillation.
FBAR = fixed-bed adsorptive reactor.

SMBR = simulated moving bed reactor.
BAc = butyl acrylate.
AAc = acrylic acid.
A15 = Amberlyst 15.
Ptz = Phenothiazine.
TCD = Thermal Conductivity Detector.
FID = Flame Ionization Detector.
DASOLV = Differential-Algebraic equation SOLVer.

Symbols

a = liquid phase activity, −
C = liquid phase concentration, mol L^{-1}.
$\overline{C}_p$ = average liquid phase concentration inside the particle, mol L^{-1}.
C_t = total liquid phase concentration, mol L^{-1}
d_p = particle diameter, cm.
$D^0_{A,B}$ = diffusion coefficient for a dilute solute A into a solvent B, $cm^2\ s^{-1}$.
$D_{A,B}$ = diffusion coefficient for binary concentrated solutions, $cm^2\ s^{-1}$
D_{ax} = axial dispersion coefficient, $cm^2\ s^{-1}$.
D_m = molecular diffusivity, $cm^2\ s^{-1}$.
K = Langmuir equilibrium parameter, L mol^{-1}
k_i = internal mass-transfer coefficient, cm s^{-1}.
k_e = external mass-transfer coefficient, cm s^{-1}.
k_c = reaction kinetic constant, mol g^{-1} min^{-1}
K_{eq} = equilibrium constant, −.
K_s = adsorption constant in Eq. 6, −.
K_L = global mass-transfer coefficient, cm s^{-1}
L_b = bed length, cm.
n = number of moles, mol.
Pe = Peclet number, −
$\overline{q}$ = average solid phase concentration in equilibrium with $\overline{C}_p$, mol L^{-1}_{res}.
Q = molar adsorption capacity ($Q_i = Q_v/V_{M,i}$) in Eq. 5, mol L^{-1}_{res}.
Q_v = volumetric monolayer capacity, L L^{-1}_{res}.
r = reaction rate, mol g^{-1} min^{-1}
r_p = particle radius, cm.
Re_p = Reynolds number relative to particle, −.
Sh_p = Sherwood number relative to particle, −
Sc = Schmidt number, −.
T = temperature, K.
$\overline{t}$ = mean residence time, min
u = interstitial velocity, cm s^{-1}.
V_M = molar volume in the liquid phase, $cm^3\ mol^{-1}$.
x = liquid phase molar fraction, −
z = fixed-bed adsorptive reactor axial coordinate, cm.

Greek letters

ε = bulk porosity, −
ε_p = catalyst/adsorbent particle porosity, −.
ζ = correction factor, −.
η = fluid viscosity, g cm^{-1} s^{-1}
η_m = mixture viscosity, g cm^{-1} s^{-1}.
ν = stoichiometric coefficient, −.
ρ = fluid phase density, g cm^{-3}
ρ_b = bulk density, g cm^{-3}.
τ = tortuosity, −.

Subscripts

exp = experimental
the = theoretical.
i = relative to component i (n-butanol, water, BAc, or AAc).
o = relative to initial conditions
F = relative to feed.
out = at the outlet of the fixed-bed column.
p = relative to particle.

Literature Cited

1. Brady FX, Kauffman TF. National Starch and Chemical Corporation. Hot melt adhesives based on ethylene-n-butyl acrylate, US 4874804, 1989.
2. Gower MD, Shanks RA. Acrylic acid level and adhesive performance and peel master-curves of acrylic pressure-sensitive adhesives. *J Polym Sci Part B: Polym Phys*. 2006;44:1237–1252.
3. Gerst M, Auchter G, Beyers CP. Basf Se. PSA polymer of n-butyl acrylate, ethyl acrylate, vinyl acrylate, and acid monomer. US 2012/0213992 A1, 2012.
4. Zeng K-L, Kuo C-L, Chien IL. Design and control of butyl acrylate reactive distillation column system. *Chem Eng Sci*. 2006;61:4417–4431.
5. OECD SIDS (Organization for Economic Cooperation and Development, Screening Information Data Set). Available at: http://www.inchem.org/documents/sids/sids/141322.pdf. Accessed May 20, 2013.
6. Pfleger K, Zacher W, Boettcher K, Skorczyk R, Buechner O, Mietzner FG. Basf Aktiengesellschaft. Manufacture of ethylene/n-butyl acrylate copolymers, US 4087601 A, 1978.
7. Chernikova EV, Yulusov VV, Garina ES, Kostina YV, Bondarenko GN, Nikolaev AY. Controlled synthesis of styrene-n-butyl acrylate copolymers with various chain microstructures mediated by dibenzyl trithiocarbonate. *Polym Sci Ser B*. 2013;55:176–186.
8. Chernikova EV, Yulusov VV, Mineeva KO, Garina ES, Sivtsov EV. Controlled synthesis of copolymers of vinyl acetate and n-butyl acrylate mediated by trithiocarbonates as reversible addition-fragmentation chain-transfer agents. *Polym Sci Ser B*. 2012;54:349–360.
9. Cooper G, Grieser F, Biggs S. Butyl acrylate/vinyl acetate copolymer latex synthesis using ultrasound as an initiator. *J Colloid Interface Sci*. 1996;184:52–63.
10. Funt BL, Ogryzlo EA. Copolymerization of butyl acrylate and vinylpyridine. *J Polym Sci*. 1957;25:279–284.
11. Niesbach A, Fuhrmeister R, Keller T, Lutze P, Górak A. Esterification of acrylic acid and n-butanol in a pilot-scale reactive distillation column—experimental investigation, model validation, and process analysis. *Ind Eng Chem Res*. 2012;51:16444–16456.
12. Niesbach A, Daniels J, Schröter B, Lutze P, Górak A. The inhibition of acrylic acid and acrylate ester polymerisation in a heterogeneously catalysed pilot-scale reactive distillation column. *Chem Eng Sci*. 2013;88:95–107.
13. Wu G, Wang C, Tan Z, Zhang H. Effect of temperature on emulsion polymerization of n-butyl acrylate. *Proc Eng*. 2011;18:353–357.
14. Mosnáček J, Nicolaÿ R, Kar KK, Fruchey SO, Cloeter MD, Harner RS, Matyjaszewski K. Efficient polymerization inhibition systems for acrylic acid distillation: new liquid-phase inhibitors. *Ind Eng Chem Res*. 2012;51:3910–3915.
15. Ohara T, Sato T, Shimizu N, Prescher G, Schwind H, Weiberg O, Marten K, Greim H. Acrylic Acid and Derivatives. *Ullmann's Encyclopedia of Industrial Chemistry*, Weinheim: Wiley-VCH Verlag GmbH & Co. KGaA, 2000.
16. Stankiewicz AI, Moulijn JA. Process intensification: Transforming chemical engineering. *Chem Eng Prog*. 2000;96:22–33.
17. Stankiewicz A. Reactive separations for process intensification: an industrial perspective. *Chem Eng Process*. 2003;42:137–144.
18. Schwarzer S, Hoffmann U. Experimental reaction equilibrium and kinetics of the liquid-phase butyl acrylate synthesis applied to reactive distillation simulations. *Chem Eng Technol*. 2002;25:975–980.
19. Niesbach A, Kuhlmann H, Keller T, Lutze P, Górak A. Optimisation of industrial-scale n-butyl acrylate production using reactive distillation. *Chem Eng Sci*. 2013;100:360–372.
20. Lode F, Mazzotti M, Morbidelli M. A new reaction-separation unit: the simulated moving bed reactor. *CHIMIA Int J Chem*. 2001;55:883–886.
21. Chen X, Xu Z, Okuhara T. Liquid phase esterification of acrylic acid with 1-butanol catalyzed by solid acid catalysts. *Appl Catal A*. 1999;180:261–269.
22. Darge O, Thyrion FC. Kinetics of the liquid phase esterification of acrylic acid with butanol catalysed by cation exchange resin. *J Chem Technol Biotechnol*. 1993;58:351–355.
23. Dupont P, Védrine JC, Paumard E, Hecquet G, Lefebvre F. Heteropolyacids supported on activated carbon as catalysts for the esterification of acrylic acid by butanol. *Appl Catal A*. 1995;129:217–227.
24. Jerzy S, Teresa W, Mirosław G, Mariusz W. Kinetics of the synthesis of propyl and butyl acrylates in the presence of some heteropolyacids as catalysts. *Int J Chem Kinet*. 2009;41:12–17.
25. Sert E, Atalay FS. Esterification of acrylic acid with different alcohols catalyzed by zirconia supported tungstophosphoric acid. *Ind Eng Chem Res*. 2012;51:6666–6671.
26. Sert E, Buluklu AD, Karakuş S, Atalay FS. Kinetic study of catalytic esterification of acrylic acid with butanol catalyzed by different ion exchange resins. *Chem Eng Process: Process Intensification*. 2013;73:23–28.
27. Ostaniewicz-Cydzik AM, Pereira CSM, Molga E, Rodrigues AE. Reaction Kinetics and Thermodynamic Equilibrium for Butyl

Acrylate Synthesis from n-Butanol and Acrylic Acid. *Ind Eng Chem Res*. 2014;53:6647–6654.
28. Pereira CSM, Silva VMTM, Rodrigues AE. Fixed bed adsorptive reactor for ethyl lactate synthesis: experiments, modelling, and simulation. *Sep Sci Technol*. 2009;44:2721–2749.
29. Mazzotti M, Kruglov A, Neri B, Gelosa D, Morbidelli M. A continuous chromatographic reactor: SMBR. *Chem Eng Sci*. 1996;51: 1827–1836.
30. Rodrigues AE, Silva VMTM. Universidade do Porto. Industrial process for acetals production in a simulated moving bed reactor. US 7488851 B2, 2009.
31. Silva VMTM, Rodrigues AE. Dynamics of a fixed-bed adsorptive reactor for synthesis of diethylacetal. *AIChE J*. 2002;48:625–634.
32. Gandi GK, Silva VMTM, Rodrigues AE. Synthesis of 1,1-dimethoxyethane in a fixed bed adsorptive reactor. *Ind Eng Chem Res*. 2006;45:2032–2039.
33. Graça NS, Pais LS, Silva VMTM, Rodrigues AE. Dynamic study of the synthesis of 1,1-dibutoxyethane in a fixed-bed adsorptive reactor. *Sep Sci Technol*. 2011;46:631–640.
34. Helfferich FG. *Ion exchange*. New York: Courier Dover Publications, 1962.
35. Sainio T, Laatikainen M, Paatero E. Phase equilibria in solvent mixture-ion exchange resin catalyst systems. *Fluid Phase Equilib*. 2004;218:269–283.
36. Pöpken T, Götze L, Gmehling J. Reaction kinetics and chemical equilibrium of homogeneously and heterogeneously catalyzed acetic acid esterification with methanol and methyl acetate hydrolysis. *Ind Eng Chem Res*. 2000;39:2601–2611.
37. Glueckauf E. Theory of chromatography. Part 10—Formulae for diffusion into spheres and their application to chromatography. *Trans Faraday Soc*. 1955;51:1540–1551.
38. Ruthven DM. *Principles of Adsorption and Adsorption Processes*. New York: Wiley, 1984.
39. Scheibel EG. Correspondence. Liquid diffusivities. Viscosity of gases. *Ind Eng Chem*. 1954;46:2007–2008.
40. Vignes A. Diffusion in binary solutions. Variation of diffusion coefficient with composition. *Ind Eng Chem Fundam*. 1966;5:189–199.
41. Perkins LR, Geankoplis CJ. Molecular diffusion in a ternary liquid system with the diffusing component dilute. *Chem Eng Sci*. 1969;24: 1035–1042.
42. Butt JB. *Reaction Kinetics and Reactor Design*. Englewood Cliffs, NJ: Prentice-Hall, 1980.
43. Ströhlein G, Assunção Y, Dube N, Bardow A, Mazzotti M, Morbidelli M. Esterification of acrylic acid with methanol by reactive chromatography: experiments and simulations. *Chem Eng Sci*. 2006;61:5296–5306.
44. Miller RG. The jackknife—a review. *Biometrika*. 1974;61:1–15.
45. Onuki Y, Nishikawa M, Morishita M, Takayama K. Development of photocrosslinked polyacrylic acid hydrogel as an adhesive for dermatological patches: involvement of formulation factors in physical properties and pharmacological effects. *Int J Pharm*. 2008;349:47–52.

Manuscript received May 7, 2014, and revision received Oct. 1, 2014.